Search for CP violation in $D^+ \to K^-K^+\pi^+$ decays

R. Aaij,[23] B. Adeva,[36] M. Adinolfi,[42] C. Adrover,[6] A. Affolder,[48] Z. Ajaltouni,[5] J. Albrecht,[37] F. Alessio,[37] M. Alexander,[47] G. Alkhazov,[29] P. Alvarez Cartelle,[36] A. A. Alves Jr,[22] S. Amato,[2] Y. Amhis,[38] J. Anderson,[39] R. B. Appleby,[50] O. Aquines Gutierrez,[10] F. Archilli,[18,37] L. Arrabito,[53] A. Artamonov,[34] M. Artuso,[52,37] E. Aslanides,[6] G. Auriemma,[22,a] S. Bachmann,[11] J. J. Back,[44] D. S. Bailey,[50] V. Balagura,[30,37] W. Baldini,[16] R. J. Barlow,[50] C. Barschel,[37] S. Barsuk,[7] W. Barter,[43] A. Bates,[47] C. Bauer,[10] Th. Bauer,[23] A. Bay,[38] I. Bediaga,[1] K. Belous,[34] I. Belyaev,[30,37] E. Ben-Haim,[8] M. Benayoun,[8] G. Bencivenni,[18] S. Benson,[46] J. Benton,[42] R. Bernet,[39] M.-O. Bettler,[17] M. van Beuzekom,[23] A. Bien,[11] S. Bifani,[12] A. Bizzeti,[17,b] P. M. Bjørnstad,[50] T. Blake,[49] F. Blanc,[38] C. Blanks,[49] J. Blouw,[11] S. Blusk,[52] A. Bobrov,[33] V. Bocci,[22] A. Bondar,[33] N. Bondar,[29] W. Bonivento,[15] S. Borghi,[47] A. Borgia,[52] T. J. V. Bowcock,[48] C. Bozzi,[16] T. Brambach,[9] J. van den Brand,[24] J. Bressieux,[38] D. Brett,[50] S. Brisbane,[51] M. Britsch,[10] T. Britton,[52] N. H. Brook,[42] H. Brown,[48] A. Büchler-Germann,[39] I. Burducea,[28] A. Bursche,[39] J. Buytaert,[37] S. Cadeddu,[15] J. M. Caicedo Carvajal,[37] O. Callot,[7] M. Calvi,[20,c] M. Calvo Gomez,[35,d] A. Camboni,[35] P. Campana,[18,37] A. Carbone,[14] G. Carboni,[21,e] R. Cardinale,[19,37,f] A. Cardini,[15] L. Carson,[36] K. Carvalho Akiba,[23] G. Casse,[48] M. Cattaneo,[37] M. Charles,[51] Ph. Charpentier,[37] N. Chiapolini,[39] K. Ciba,[37] X. Cid Vidal,[36] G. Ciezarek,[49] P. E. L. Clarke,[46,37] M. Clemencic,[37] H. V. Cliff,[43] J. Closier,[37] C. Coca,[28] V. Coco,[23] J. Cogan,[6] P. Collins,[37] F. Constantin,[28] G. Conti,[38] A. Contu,[51] A. Cook,[42] M. Coombes,[42] G. Corti,[37] G. A. Cowan,[38] R. Currie,[46] B. D'Almagne,[7] C. D'Ambrosio,[37] P. David,[8] I. De Bonis,[4] S. De Capua,[21,e] M. De Cian,[39] F. De Lorenzi,[12] J. M. De Miranda,[1] L. De Paula,[2] P. De Simone,[18] D. Decamp,[4] M. Deckenhoff,[9] H. Degaudenzi,[38,37] M. Deissenroth,[11] L. Del Buono,[8] C. Deplano,[15] O. Deschamps,[5] F. Dettori,[15,g] J. Dickens,[43] H. Dijkstra,[37] P. Diniz Batista,[1] S. Donleavy,[48] F. Dordei,[11] A. Dosil Suárez,[36] D. Dossett,[44] A. Dovbnya,[40] F. Dupertuis,[38] R. Dzhelyadin,[34] C. Eames,[49] S. Easo,[45] U. Egede,[49] V. Egorychev,[30] S. Eidelman,[33] D. van Eijk,[23] F. Eisele,[11] S. Eisenhardt,[46] R. Ekelhof,[9] L. Eklund,[47] Ch. Elsasser,[39] D. G. d'Enterria,[35,h] D. Esperante Pereira,[36] L. Estève,[43] A. Falabella,[16,i] E. Fanchini,[20,c] C. Färber,[11] G. Fardell,[46] C. Farinelli,[23] S. Farry,[12] V. Fave,[38] V. Fernandez Albor,[36] M. Ferro-Luzzi,[37] S. Filippov,[32] C. Fitzpatrick,[46] M. Fontana,[10] F. Fontanelli,[19,f] R. Forty,[37] M. Frank,[37] C. Frei,[37] M. Frosini,[17,37,j] S. Furcas,[20] A. Gallas Torreira,[36] D. Galli,[14,k] M. Gandelman,[2] P. Gandini,[51] Y. Gao,[3] J-C. Garnier,[37] J. Garofoli,[52] J. Garra Tico,[43] L. Garrido,[35] C. Gaspar,[37] N. Gauvin,[38] M. Gersabeck,[37] T. Gershon,[44,37] Ph. Ghez,[4] V. Gibson,[43] V. V. Gligorov,[37] C. Göbel,[54,q] D. Golubkov,[30] A. Golutvin,[49,30,37] A. Gomes,[2] H. Gordon,[51] M. Grabalosa Gándara,[35] R. Graciani Diaz,[35] L. A. Granado Cardoso,[37] E. Graugés,[35] G. Graziani,[17] A. Grecu,[28] S. Gregson,[43] B. Gui,[52] E. Gushchin,[32] Yu. Guz,[34] T. Gys,[37] G. Haefeli,[38] C. Haen,[37] S. C. Haines,[43] T. Hampson,[42] S. Hansmann-Menzemer,[11] R. Harji,[49] N. Harnew,[51] J. Harrison,[50] P. F. Harrison,[44] J. He,[7] V. Heijne,[23] K. Hennessy,[48] P. Henrard,[5] J. A. Hernando Morata,[36] E. van Herwijnen,[37] E. Hicks,[48] W. Hofmann,[10] K. Holubyev,[11] P. Hopchev,[4] W. Hulsbergen,[23] P. Hunt,[51] T. Huse,[48] R. S. Huston,[12] D. Hutchcroft,[48] D. Hynds,[47] V. Iakovenko,[41] P. Ilten,[12] J. Imong,[42] R. Jacobsson,[37] A. Jaeger,[11] M. Jahjah Hussein,[5] E. Jans,[23] F. Jansen,[23] P. Jaton,[38] B. Jean-Marie,[7] F. Jing,[3] M. John,[51] D. Johnson,[51] C. R. Jones,[43] B. Jost,[37] S. Kandybei,[40] M. Karacson,[37] T. M. Karbach,[9] J. Keaveney,[12] U. Kerzel,[37] T. Ketel,[24] A. Keune,[38] B. Khanji,[6] Y. M. Kim,[46] M. Knecht,[38] S. Koblitz,[37] P. Koppenburg,[23] A. Kozlinskiy,[23] L. Kravchuk,[32] K. Kreplin,[11] M. Kreps,[44] G. Krocker,[11] P. Krokovny,[11] F. Kruse,[9] K. Kruzelecki,[37] M. Kucharczyk,[20,25,37] S. Kukulak,[25] R. Kumar,[14,37] T. Kvaratskheliya,[30,37] V. N. La Thi,[38] D. Lacarrere,[37] G. Lafferty,[50] A. Lai,[15] D. Lambert,[46] R. W. Lambert,[37] E. Lanciotti,[37] G. Lanfranchi,[18] C. Langenbruch,[11] T. Latham,[44] R. Le Gac,[6] J. van Leerdam,[23] J.-P. Lees,[4] R. Lefèvre,[5] A. Leflat,[31,37] J. Lefrançois,[7] O. Leroy,[6] T. Lesiak,[25] L. Li,[3] L. Li Gioi,[5] M. Lieng,[9] M. Liles,[48] R. Lindner,[37] C. Linn,[11] B. Liu,[3] G. Liu,[37] J. H. Lopes,[2] E. Lopez Asamar,[35] N. Lopez-March,[38] J. Luisier,[38] F. Machefert,[7] I. V. Machikhiliyan,[4,30] F. Maciuc,[10] O. Maev,[29,37] J. Magnin,[1] S. Malde,[51] R. M. D. Mamunur,[37] G. Manca,[15,g] G. Mancinelli,[6] N. Mangiafave,[43] U. Marconi,[14] R. Märki,[38] J. Marks,[11] G. Martellotti,[22] A. Martens,[7] L. Martin,[51] A. Martín Sánchez,[7] D. Martinez Santos,[37] D. Martins Tostes,[1] A. Massafferri,[1] Z. Mathe,[12] C. Matteuzzi,[20] M. Matveev,[29] E. Maurice,[6] B. Maynard,[52] A. Mazurov,[16,32,37] G. McGregor,[50] R. McNulty,[12] C. Mclean,[14] M. Meissner,[11] M. Merk,[23] J. Merkel,[9] R. Messi,[21,e] S. Miglioranzi,[37] D. A. Milanes,[13,37] M.-N. Minard,[4] J. Molina Rodriguez,[54,q] S. Monteil,[5] D. Moran,[12] P. Morawski,[25] R. Mountain,[52] I. Mous,[23] F. Muheim,[46] K. Müller,[39] R. Muresan,[28,38] B. Muryn,[26] M. Musy,[35] J. Mylroie-Smith,[48] P. Naik,[42] T. Nakada,[38] R. Nandakumar,[45] J. Nardulli,[45] I. Nasteva,[1] M. Nedos,[9] M. Needham,[46] N. Neufeld,[37] C. Nguyen-Mau,[38,l] M. Nicol,[7] S. Nies,[9] V. Niess,[5] N. Nikitin,[31] A. Oblakowska-Mucha,[26] V. Obraztsov,[34] S. Oggero,[23] S. Ogilvy,[47] O. Okhrimenko,[41] R. Oldeman,[15,g] M. Orlandea,[28] J. M. Otalora Goicochea,[2] P. Owen,[49] B. Pal,[52] J. Palacios,[39] M. Palutan,[18] J. Panman,[37] A. Papanestis,[45] M. Pappagallo,[13,m] C. Parkes,[47,37] C. J. Parkinson,[49] G. Passaleva,[17] G. D. Patel,[48] M. Patel,[49] S. K. Paterson,[49] G. N. Patrick,[45] C. Patrignani,[19,f] C. Pavel-Nicorescu,[28]

A. Pazos Alvarez,[36] A. Pellegrino,[23] G. Penso,[22,n] M. Pepe Altarelli,[37] S. Perazzini,[14,k] D. L. Perego,[20,c] E. Perez Trigo,[36] A. Pérez-Calero Yzquierdo,[35] P. Perret,[5] M. Perrin-Terrin,[6] G. Pessina,[20] A. Petrella,[16,37] A. Petrolini,[19,f] B. Pie Valls,[35] B. Pietrzyk,[4] T. Pilar,[44] D. Pinci,[22] R. Plackett,[47] S. Playfer,[46] M. Plo Casasus,[36] G. Polok,[25] A. Poluektov,[44,33] E. Polycarpo,[2] D. Popov,[10] B. Popovici,[28] C. Potterat,[35] A. Powell,[51] T. du Pree,[23] J. Prisciandaro,[38] V. Pugatch,[41] A. Puig Navarro,[35] W. Qian,[52] J. H. Rademacker,[42] B. Rakotomiaramanana,[38] M. S. Rangel,[2] I. Raniuk,[40] G. Raven,[24] S. Redford,[51] M. M. Reid,[44] A. C. dos Reis,[1] S. Ricciardi,[45] K. Rinnert,[48] D. A. Roa Romero,[5] P. Robbe,[7] E. Rodrigues,[47] F. Rodrigues,[2] P. Rodriguez Perez,[36] G. J. Rogers,[43] S. Roiser,[37] V. Romanovsky,[34] J. Rouvinet,[38] T. Ruf,[37] H. Ruiz,[35] G. Sabatino,[21,e] J. J. Saborido Silva,[36] N. Sagidova,[29] P. Sail,[47] B. Saitta,[15,g] C. Salzmann,[39] M. Sannino,[19,f] R. Santacesaria,[22] C. Santamarina Rios,[36] R. Santinelli,[37] E. Santovetti,[21,e] M. Sapunov,[6] A. Sarti,[18,n] C. Satriano,[22,a] A. Satta,[21] M. Savrie,[16,i] D. Savrina,[30] P. Schaack,[49] M. Schiller,[11] S. Schleich,[9] M. Schmelling,[10] B. Schmidt,[37] O. Schneider,[38] A. Schopper,[37] M.-H. Schune,[7] R. Schwemmer,[37] A. Sciubba,[18,n] M. Seco,[36] A. Semennikov,[30] K. Senderowska,[26] I. Sepp,[49] N. Serra,[39] J. Serrano,[6] P. Seyfert,[11] B. Shao,[3] M. Shapkin,[34] I. Shapoval,[40,37] P. Shatalov,[30] Y. Shcheglov,[29] T. Shears,[48] L. Shekhtman,[33] O. Shevchenko,[40] V. Shevchenko,[30] A. Shires,[49] R. Silva Coutinho,[54,q] H. P. Skottowe,[43] T. Skwarnicki,[52] A. C. Smith,[37] N. A. Smith,[48] K. Sobczak,[5] F. J. P. Soler,[47] A. Solomin,[42] F. Soomro,[49] B. Souza De Paula,[2] B. Spaan,[9] A. Sparkes,[46] P. Spradlin,[47] F. Stagni,[37] S. Stahl,[11] O. Steinkamp,[39] S. Stoica,[28] S. Stone,[52,37] B. Storaci,[23] M. Straticiuc,[28] U. Straumann,[39] N. Styles,[46] V. K. Subbiah,[37] S. Swientek,[9] M. Szczekowski,[27] P. Szczypka,[38] T. Szumlak,[26] S. T'Jampens,[4] E. Teodorescu,[28] F. Teubert,[37] C. Thomas,[51,45] E. Thomas,[37] J. van Tilburg,[11] V. Tisserand,[4] M. Tobin,[39] S. Topp-Joergensen,[51] M. T. Tran,[38] A. Tsaregorodtsev,[6] N. Tuning,[23] M. Ubeda Garcia,[37] A. Ukleja,[27] P. Urquijo,[52] U. Uwer,[11] V. Vagnoni,[14] G. Valenti,[14] R. Vazquez Gomez,[35] P. Vazquez Regueiro,[36] S. Vecchi,[16] J. J. Velthuis,[42] M. Veltri,[17,o] K. Vervink,[37] B. Viaud,[7] I. Videau,[7] D. Vieira,[2] X. Vilasis-Cardona,[35,d] J. Visniakov,[36] A. Vollhardt,[39] D. Voong,[42] A. Vorobyev,[29] H. Voss,[10] K. Wacker,[9] S. Wandernoth,[11] J. Wang,[52] D. R. Ward,[43] A. D. Webber,[50] D. Websdale,[49] M. Whitehead,[44] D. Wiedner,[11] L. Wiggers,[23] G. Wilkinson,[51] M. P. Williams,[44,45] M. Williams,[49] F. F. Wilson,[45] J. Wishahi,[9] M. Witek,[25,37] W. Witzeling,[37] S. A. Wotton,[43] K. Wyllie,[37] Y. Xie,[46] F. Xing,[51] Z. Yang,[3] R. Young,[46] O. Yushchenko,[34] M. Zavertyaev,[10,p] F. Zhang,[3] L. Zhang,[52] W. C. Zhang,[12] Y. Zhang,[3] A. Zhelezov,[11] L. Zhong,[3] E. Zverev,[31] and A. Zvyagin[37]

(LHCb Collaboration)

[1]*Centro Brasileiro de Pesquisas Físicas (CBPF), Rio de Janeiro, Brazil*
[2]*Universidade Federal do Rio de Janeiro (UFRJ), Rio de Janeiro, Brazil*
[3]*Center for High Energy Physics, Tsinghua University, Beijing, China*
[4]*LAPP, Université de Savoie, CNRS/IN2P3, Annecy-Le-Vieux, France*
[5]*Clermont Université, Université Blaise Pascal, CNRS/IN2P3, LPC, Clermont-Ferrand, France*
[6]*CPPM, Aix-Marseille Université, CNRS/IN2P3, Marseille, France*
[7]*LAL, Université Paris-Sud, CNRS/IN2P3, Orsay, France*
[8]*LPNHE, Université Pierre et Marie Curie, Université Paris Diderot, CNRS/IN2P3, Paris, France*

[a]Università della Basilicata, Potenza, Italy
[b]Università di Modena e Reggio Emilia, Modena, Italy
[c]Università di Milano Bicocca, Milano, Italy
[d]LIFAELS, La Salle, Universitat Ramon Llull, Barcelona, Spain
[e]Università di Roma Tor Vergata, Roma, Italy
[f]Università di Genova, Genova, Italy
[g]Università di Cagliari, Cagliari, Italy
[h]Institució Catalana de Recerca i Estudis Avançats (ICREA), Barcelona, Spain
[i]Università di Ferrara, Ferrara, Italy
[j]Università di Firenze, Firenze, Italy
[k]Università di Bologna, Bologna, Italy
[l]Hanoi University of Science, Hanoi, Viet Nam
[m]Università di Bari, Bari, Italy
[n]Università di Roma La Sapienza, Roma, Italy
[o]Università di Urbino, Urbino, Italy
[p]P.N. Lebedev Physical Institute, Russian Academy of Science (LPI RAS), Moscow, Russia
[q]Associated to Universidade Federal do Rio de Janeiro (UFRJ), Rio de Janeiro, Brazil

[9]*Fakultät Physik, Technische Universität Dortmund, Dortmund, Germany*
[10]*Max-Planck-Institut für Kernphysik (MPIK), Heidelberg, Germany*
[11]*Physikalisches Institut, Ruprecht-Karls-Universität Heidelberg, Heidelberg, Germany*
[12]*School of Physics, University College Dublin, Dublin, Ireland*
[13]*Sezione INFN di Bari, Bari, Italy*
[14]*Sezione INFN di Bologna, Bologna, Italy*
[15]*Sezione INFN di Cagliari, Cagliari, Italy*
[16]*Sezione INFN di Ferrara, Ferrara, Italy*
[17]*Sezione INFN di Firenze, Firenze, Italy*
[18]*Laboratori Nazionali dell'INFN di Frascati, Frascati, Italy*
[19]*Sezione INFN di Genova, Genova, Italy*
[20]*Sezione INFN di Milano Bicocca, Milano, Italy*
[21]*Sezione INFN di Roma Tor Vergata, Roma, Italy*
[22]*Sezione INFN di Roma La Sapienza, Roma, Italy*
[23]*Nikhef National Institute for Subatomic Physics, Amsterdam, Netherlands*
[24]*Nikhef National Institute for Subatomic Physics and Vrije Universiteit, Amsterdam, Netherlands*
[25]*Henryk Niewodniczanski Institute of Nuclear Physics Polish Academy of Sciences, Cracow, Poland*
[26]*Faculty of Physics & Applied Computer Science, Cracow, Poland*
[27]*Soltan Institute for Nuclear Studies, Warsaw, Poland*
[28]*Horia Hulubei National Institute of Physics and Nuclear Engineering, Bucharest-Magurele, Romania*
[29]*Petersburg Nuclear Physics Institute (PNPI), Gatchina, Russia*
[30]*Institute of Theoretical and Experimental Physics (ITEP), Moscow, Russia*
[31]*Institute of Nuclear Physics, Moscow State University (SINP MSU), Moscow, Russia*
[32]*Institute for Nuclear Research of the Russian Academy of Sciences (INR RAN), Moscow, Russia*
[33]*Budker Institute of Nuclear Physics (SB RAS) and Novosibirsk State University, Novosibirsk, Russia*
[34]*Institute for High Energy Physics (IHEP), Protvino, Russia*
[35]*Universitat de Barcelona, Barcelona, Spain*
[36]*Universidad de Santiago de Compostela, Santiago de Compostela, Spain*
[37]*European Organization for Nuclear Research (CERN), Geneva, Switzerland*
[38]*Ecole Polytechnique Fédérale de Lausanne (EPFL), Lausanne, Switzerland*
[39]*Physik-Institut, Universität Zürich, Zürich, Switzerland*
[40]*NSC Kharkiv Institute of Physics and Technology (NSC KIPT), Kharkiv, Ukraine*
[41]*Institute for Nuclear Research of the National Academy of Sciences (KINR), Kyiv, Ukraine*
[42]*H.H. Wills Physics Laboratory, University of Bristol, Bristol, United Kingdom*
[43]*Cavendish Laboratory, University of Cambridge, Cambridge, United Kingdom*
[44]*Department of Physics, University of Warwick, Coventry, United Kingdom*
[45]*STFC Rutherford Appleton Laboratory, Didcot, United Kingdom*
[46]*School of Physics and Astronomy, University of Edinburgh, Edinburgh, United Kingdom*
[47]*School of Physics and Astronomy, University of Glasgow, Glasgow, United Kingdom*
[48]*Oliver Lodge Laboratory, University of Liverpool, Liverpool, United Kingdom*
[49]*Imperial College London, London, United Kingdom*
[50]*School of Physics and Astronomy, University of Manchester, Manchester, United Kingdom*
[51]*Department of Physics, University of Oxford, Oxford, United Kingdom*
[52]*Syracuse University, Syracuse, New York, United States*
[53]*CC-IN2P3, CNRS/IN2P3, Lyon-Villeurbanne, France, associated member*
[54]*Pontifícia Universidade Católica do Rio de Janeiro (PUC-Rio), Rio de Janeiro, Brazil*
(Received 18 October 2011; published 28 December 2011)

A model-independent search for direct *CP* violation in the Cabibbo-suppressed decay $D^+ \to K^- K^+ \pi^+$ in a sample of approximately 370 000 decays is carried out. The data were collected by the LHCb experiment in 2010 and correspond to an integrated luminosity of 35 pb^{-1}. The normalized Dalitz plot distributions for D^+ and D^- are compared using four different binning schemes that are sensitive to different manifestations of *CP* violation. No evidence for *CP* asymmetry is found.

DOI: 10.1103/PhysRevD.84.112008 PACS numbers: 13.25.Ft, 11.30.Er, 14.40.Lb

I. INTRODUCTION

To date *CP* violation (CPV) has been observed only in decays of neutral K and B mesons. All observations are consistent with CPV being generated by the phase in the

Cabibbo-Kobayashi-Maskawa matrix [1,2] of the standard model. In the charm sector, Cabibbo-Kobayashi-Maskawa dynamics can produce direct *CP* asymmetries in Cabibbo-suppressed $D^{\pm}$ decays of the order of 10^{-3} or less [3]. Asymmetries of up to around 1% can be generated by new physics [4,5]. In most extensions of the standard model, asymmetries arise in processes with loop diagrams. However, in some cases CPV could occur even at tree level, for example, in models with charged Higgs exchange.

In decays of hadrons, CPV can be observed when two different amplitudes with nonzero relative weak and strong phases contribute coherently to a final state. Three-body decays are dominated by intermediate resonant states, and the requirement of a nonzero relative strong phase is fulfilled by the phases of the resonances. In two-body decays, CPV leads to an asymmetry in the partial widths. In three-body decays, the interference between resonances in the two-dimensional phase space can lead to observable asymmetries which vary across the Dalitz plot.

CP-violating phase differences of 10° or less do not, in general, lead to large asymmetries in integrated decay rates, but they could have clear signatures in the Dalitz plot, as we will show in Sec. III. This means that a two-dimensional search should have higher sensitivity than an integrated measurement. In addition, the distribution of an asymmetry across phase space could hint at the underlying dynamics.

At present, no theoretical tools for computing decay fractions and relative phases of resonant modes in D decays have been applied to multibody D^+ decay modes, and no predictions have been made for how asymmetries might vary across their Dalitz plots. A full Dalitz plot analysis of large data samples could, in principle, measure small phase differences. However, rigorous control of the much larger strong phases would be required. For this to be achieved, better understanding of the amplitudes, especially in the scalar sector, will be needed, and effects like three-body final state interactions should be taken into account.

This paper describes a model-independent search for direct CPV in the Cabibbo-suppressed decay $D^+ \to K^-K^+\pi^+$ in a binned Dalitz plot [6]. A direct comparison between the D^+ and the D^- Dalitz plots is made on a bin-by-bin basis. The data sample used is approximately 35 pb^{-1} collected in 2010 by the LHCb experiment at a center of mass energy of $\sqrt{s} = 7$ TeV. This data set corresponds to nearly 10 and 20 times more signal events than used in previous studies of this channel performed by the *BABAR* [7] and CLEO-c [8] collaborations, respectively. It is comparable to the data set used in a more recent search for CPV in $D^+ \to \phi\pi^+$ decays at BELLE [9].

The strategy is as follows. For each bin in the Dalitz plot, a local *CP* asymmetry variable is defined [10,11],

$$\mathcal{S}^{i}_{CP} = \frac{N^i(D^+) - \alpha N^i(D^-)}{\sqrt{N^i(D^+) + \alpha^2 N^i(D^-)}}, \quad \alpha = \frac{N_{\rm tot}(D^+)}{N_{\rm tot}(D^-)}, \qquad (1)$$

where $N^i(D^+)$ and $N^i(D^-)$ are the numbers of $D^{\pm}$ candidates in the ith bin and α is the ratio between the total D^+ and D^- yields. The parameter α accounts for global asymmetries, i.e. those that are constant across the Dalitz plot.

In the absence of Dalitz plot-dependent asymmetries, the $\mathcal{S}^i_{CP}$ values are distributed according to a Gaussian distribution with zero mean and unit width. CPV signals are, therefore, deviations from this behavior. The numerical comparison between the D^+ and the D^- Dalitz plots is made with a χ^2 test ($\chi^2 = \sum(\mathcal{S}^i_{CP})^2$). The number of degrees of freedom is the number of bins minus one (due to the constraint of the overall D^+/D^- normalization). The p-value that results from this test is defined as the probability of obtaining, for a given number of degrees of freedom and under the assumption of no CPV, a χ^2 that is at least as high as the value observed [12]. It measures the degree to which we are confident that the differences between the D^+ and D^- Dalitz plots are driven only by statistical fluctuations.

If CPV is observed, the p-value from this test could be converted into a significance for a signal using Gaussian statistics. However, in the event that no CPV is found, there is no model-independent mechanism for setting limits on CPV within this procedure. In this case, the results can be compared to simulation studies in which an artificial *CP* asymmetry is introduced into an assumed amplitude model for the decay. Since such simulations are clearly model-dependent, they are only used as a guide to the sensitivity of the method, and not in the determination of the p-values that constitute the results of the analysis.

The technique relies on careful accounting for local asymmetries that could be induced by sources such as, the difference in the K–nucleon inelastic cross section, differences in the reconstruction or trigger efficiencies, left-right detector asymmetries, etc. These effects are investigated in the two control channels $D^+ \to K^-\pi^+\pi^+$ and $D_s^+ \to K^-K^+\pi^+$.

The optimum sensitivity is obtained with bins of nearly the same size as the area over which the asymmetry extends in the Dalitz plot. Since this is a search for new and therefore unknown phenomena, it is necessary to be sensitive to effects restricted to small areas as well as those that extend over a large region of the Dalitz plot. Therefore two types of binning scheme are employed. The first type is simply a uniform grid of equally sized bins. The second type takes into account the fact that the $D^+ \to K^-K^+\pi^+$ Dalitz plot is dominated by the $\phi\pi^+$ and $\bar{K}^*(892)^0K^+$ resonances, so the event distribution is highly nonuniform. This ''adaptive binning'' scheme uses smaller bins where the density of events is high, aiming for a uniform bin population. In each scheme, different numbers of bins are used in our search for localized asymmetries.

The paper is organized as follows. In Sec. II, a description of the LHCb experiment and of the data selection

is presented. In Sec. III, the methods and the binnings are discussed in detail. The study of the control channels and of possible asymmetries generated by detector effects or backgrounds is presented in Sec. IV. The results of our search are given in Sec. V, and the conclusions in Sec. VI.

II. DETECTOR, DATA SET AND SELECTION

The LHCb detector [13] is a single-arm forward spectrometer with the main purpose of measuring CPV and rare decays of hadrons containing b and c quarks. A vertex locator determines with high precision the positions of the vertices of primary pp collisions (PVs) and the decay vertices of long-lived particles. The tracking system also includes a large area silicon strip detector located in front of a dipole magnet with an integrated field of around 4 Tm, and a combination of silicon strip detectors and straw drift chambers placed behind the magnet. Charged hadron identification is achieved with two ring-imaging Cherenkov (RICH) detectors. The calorimeter system consists of a preshower, a scintillator pad detector, an electromagnetic calorimeter and a hadronic calorimeter. It identifies high transverse energy (E_T) hadron, electron and photon candidates and provides information for the trigger. Five muon stations composed of multiwire proportional chambers and triple gas electron multipliers provide fast information for the trigger and muon identification capability.

The LHCb trigger consists of two levels. The first, hardware-based level selects leptonic and hadronic final states with high transverse momentum, using the subset of the detectors that are able to reduce the rate at which the whole detector is read out to a maximum of 1 MHz. The second level, the high level trigger (HLT), is subdivided into two software stages that can use the information from all parts of the detector. The first stage, HLT1, performs a partial reconstruction of the event, reducing the rate further and allowing the next stage, HLT2, to fully reconstruct the individual channels. At each stage, several selections designed for specific types of decay exist. As luminosity increased throughout 2010 several changes in the trigger were required. To match these, the data sets for signal and control modes are divided into three parts according to the trigger, samples 1, 2 and 3, which correspond to integrated luminosities of approximately 3, 5 and 28 pb^{-1}, respectively. The magnet polarity was changed several times during data taking.

The majority of the signal decays come via the hadronic hardware trigger, which has an E_T threshold that varied between 2.6 and 3.6 GeV in 2010. In the HLT1, most candidates also come from the hadronic selections which retain events with at least one high transverse momentum (p_T) track that is displaced from the PV. In the HLT2, dedicated charm triggers select most of the signal. However, the signal yield for these channels can be increased by using other trigger selections, such as those for decays of the form $B \to DX$. To maintain the necessary control of Dalitz plot-dependent asymmetries, only events from selections which have been measured not to introduce charge asymmetries into the Dalitz plot of the $D^+ \to K^-\pi^+\pi^+$ control mode are accepted.

The signal ($D^+ \to K^-K^+\pi^+$) and control ($D^+ \to K^-\pi^+\pi^+$ and $D_s^+ \to K^-K^+\pi^+$) mode candidates are selected using the same criteria, which are chosen to maximize the statistical significance of the signal. Moreover, care is taken to use selection cuts that do not have a low efficiency in any part of the Dalitz plot, as this would reduce the sensitivity in these areas. The selection criteria are the same regardless of the trigger conditions.

The event selection starts by requiring at least one PV with a minimum of five charged tracks to exist. To control CPU consumption each event must also have fewer than 350 reconstructed tracks. The particle identification system constructs a relative log-likelihood for pion and kaon hypotheses, $\text{DLL}_{K\pi}$, and we require $\text{DLL}_{K\pi} > 7$ for kaons and <3 for pions. Three particles with appropriate charges are combined to form the $D^+_{(s)}$ candidates. The corresponding tracks are required to have a good fit quality ($\chi^2/\text{ndf} < 5$), $p_T > 250$ MeV/c, momentum $p > 2000$ MeV/c and the scalar sum of their p_T above 2800 MeV/c. Because a typical D^+ travels for around 8 mm before decaying, the final state tracks should not point to the PV. The smallest displacement from each track to the PV is computed, and a χ^2 (χ^2_{IP}), formed by using the hypothesis that this distance is equal to zero, is required to be greater than 4 for each track. The three daughters should be produced at a common origin, the charm decay vertex, with vertex fit $\chi^2/\text{ndf} < 10$.

This "secondary" vertex must be well separated from any PV, thus a flight distance variable (χ^2_{FD}) is constructed. The secondary vertex is required to have $\chi^2_{\text{FD}} > 100$, and to be downstream of the PV. The p_T of the $D^+_{(s)}$ candidate must be greater than 1000 MeV/c, and its reconstructed trajectory is required to originate from the PV ($\chi^2_{\text{IP}} < 12$).

In order to quantify the signal yields (S), a simultaneous fit to the invariant mass distribution of the D^+ and D^- samples is performed. A double Gaussian is used for the $K^-K^+\pi^+$ signal, while the background (B) is described by a quadratic component and a single Gaussian for the small contamination from $D^{*+} \to D^0(K^-K^+)\pi^+$ above the D_s^+ peak. The fitted mass spectrum for samples 1 and 3 combined is shown in Fig. 1, giving the yields shown in Table I. A weighted mean of the widths of the two Gaussian contributions to the mass peaks is used to determine the overall widths, σ, as 6.35 MeV/c^2 for $D^+ \to K^-K^+\pi^+$, 7.05 MeV/c^2 for $D_s^+ \to K^-K^+\pi^+$, and 8.0 MeV/c^2 for $D^+ \to K^-\pi^+\pi^+$. These values are used to define signal mass windows of approximately 2σ in which the Dalitz plots are constructed. The purities, defined as $S/(B+S)$ within these mass regions, are also shown in Table I for samples 1 and 3 in the different decay modes.

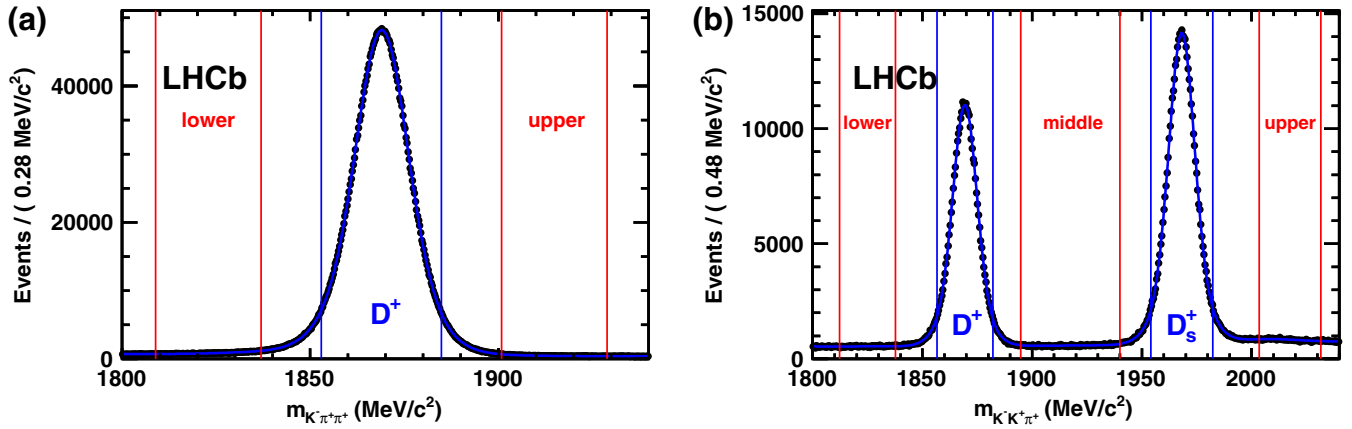

FIG. 1 (color online). Fitted mass spectra of (a) $K^-\pi^+\pi^+$ and (b) $K^-K^+\pi^+$ candidates from samples 1 and 3, D^+ and D^- combined. The signal mass windows and sidebands defined in the text are labeled.

For sample 2, the yield cannot be taken directly from the fit, because there is a mass cut in the HLT2 line that accepts the majority of the signal, selecting events in a $\pm 25\ \mathrm{MeV}/c^2$ window around the nominal value. However, another HLT2 line with a looser mass cut that is otherwise identical to the main HLT2 line exists, although only one event in 100 is retained. In this line the purity is found to be the same in sample 2 as in sample 3. The yield in sample 2 is then inferred as the total $(S + B)$ in all allowed triggers in the mass window times the purity in sample 3. Thus the overall yield of signal $D^+ \to K^-K^+\pi^+$ candidates in the three samples within the mass window is approximately 370 000. The total number of candidates $(S + B)$ in each decay mode used in the analysis are given in Table II. The Dalitz plot of data in the D^+ window is shown in Fig. 2.

TABLE I. Yield (S) and purity for samples 1 and 3 after the final selection. The purity is estimated in the 2σ mass window.

Decay	Yield	Purity	
	Sample 1 + 3	Sample 1	Sample 3
$D^+ \to K^-K^+\pi^+$	$(3.284 \pm 0.006) \times 10^5$	88%	92%
$D_s^+ \to K^-K^+\pi^+$	$(4.615 \pm 0.012) \times 10^5$	89%	92%
$D^+ \to K^-\pi^+\pi^+$	$(3.3777 \pm 0.0037) \times 10^6$	98%	98%

TABLE II. Number of candidates $(S + B)$ in the signal windows shown in Fig. 1 after the final selection, for use in the subsequent analysis.

	Sample 1	Sample 2	Sample 3	Total
$D^+ \to K^-K^+\pi^+$	84 667	65 781	253 446	403 894
$D_s^+ \to K^-K^+\pi^+$	126 206	91 664	346 068	563 938
$D^+ \to K^-\pi^+\pi^+$	858 356	687 197	2 294 315	3 839 868

Within the 2σ $D^+ \to K^-K^+\pi^+$ mass window, about 8.6% of events are background. Apart from random three-body track combinations, charm backgrounds and two-body resonances plus one track are expected. Charm reflections appear when a particle is wrongly identified in a true charm three-body decay and/or a track in a four-body charm decay is lost. The main three-body reflection in the $K^-K^+\pi^+$ spectrum is the Cabibbo-favored $D^+ \to K^-\pi^+\pi^+$, where the incorrect assignment of the kaon mass to the pion leads to a distribution that partially overlaps with the $D_s^+ \to K^-K^+\pi^+$ signal region, but not with $D^+ \to K^-K^+\pi^+$. The four-body, Cabibbo-favored mode $D^0 \to K^-\pi^+\pi^-\pi^+$ where a π^+ is lost and the π^- is misidentified as a K^- will appear broadly distributed in $K^-K^+\pi^+$ mass, but its resonances could create structures in the Dalitz plot. Similarly, $\bar{K}^*(892)^0$ and ϕ resonances from the PV misreconstructed with a random track forming a three-body vertex will also appear.

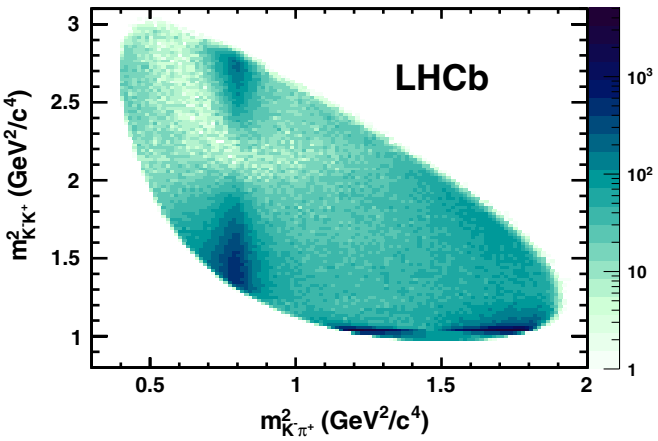

FIG. 2 (color online). Dalitz plot of the $D^+ \to K^-K^+\pi^+$ decay for selected candidates in the signal window. The vertical $\bar{K}^*(892)^0$ and horizontal $\phi(1020)$ contributions are clearly visible in the data.

TABLE III. The CLEO-c amplitude model "B" [8] used in the simulation studies. The uncertainties are statistical, experimental systematic and model systematic, respectively.

Resonance	Amplitude	Relative phase	Fit fraction
$\bar{K}^*(892)^0$	1 (fixed)	0 (fixed)	$25.7 \pm 0.5^{+0.4+0.1}_{-0.3-1.2}$
$\bar{K}_0^*(1430)^0$	$4.56 \pm 0.13^{+0.10+0.42}_{-0.01-0.39}$	$70 \pm 6^{+1+16}_{-6-23}$	$18.8 \pm 1.2^{+0.6+3.2}_{-0.1-3.4}$
$\kappa(800)$	$2.30 \pm 0.13^{+0.01+0.52}_{-0.11-0.29}$	$-87 \pm 6^{+2+15}_{-3-10}$	$7.0 \pm 0.8^{+0.0+3.5}_{-0.6-1.9}$
$\bar{K}_2^*(1430)^0$	$7.6 \pm 0.8^{+0.5+2.4}_{-0.6-4.8}$	$171 \pm 4^{+0+24}_{-2-11}$	$1.7 \pm 0.4^{+0.3+1.2}_{-0.2-0.7}$
$\phi(1020)$	$1.166 \pm 0.015^{+0.001+0.025}_{-0.009-0.009}$	$-163 \pm 3^{+1+14}_{-1-5}$	$27.8 \pm 0.4^{+0.1+0.2}_{-0.3-0.4}$
$a_0(1450)^0$	$1.50 \pm 0.10^{+0.09+0.92}_{-0.06-0.33}$	$116 \pm 2^{+1+7}_{-1-14}$	$4.6 \pm 0.6^{+0.5+7.2}_{-0.3-1.8}$
$\phi(1680)$	$1.86 \pm 0.20^{+0.02+0.62}_{-0.08-0.77}$	$-112 \pm 6^{+3+19}_{-4-12}$	$0.51 \pm 0.11^{+0.01+0.37}_{-0.04-0.15}$

III. METHODS AND BINNINGS

Monte Carlo pseudo-experiments are used to verify that we can detect CPV with the strategy outlined in Sec. I without producing fake signals, and to devise and test suitable binning schemes for the Dalitz plot. They are also used to quantify our sensitivity to possible manifestations of CPV, where we define the sensitivity to a given level of CPV as the probability of observing it with 3σ significance.

For the $D^+ \to K^-K^+\pi^+$ Dalitz plot model, the result of the CLEO-c analysis (fit B) [8] is used. The amplitudes and phases of the resonances used in this model are reproduced in Table III. For simplicity, only resonant modes with fit fractions greater than 2% are included in the pseudo-experiments. The fit fraction for a resonance is defined as the integral of its squared amplitude over the Dalitz plot divided by the integral of the square of the overall complex amplitude. An efficiency function is determined from a two-dimensional second order polynomial fit to the Dalitz plot distribution of triggered events that survive the selection cuts in the GEANT-based [14] LHCb Monte Carlo simulation for nonresonant $D^+ \to K^-K^+\pi^+$. A simple model for the background is inferred from the Dalitz plots of the sidebands of the $D^+ \to K^-K^+\pi^+$ signal. It is composed of random combinations of K^-, K^+, and π^+ tracks, ϕ resonances with π^+ tracks, and $\bar{K}^*(892)^0$ resonances with K^+ tracks. The CLEO-c Dalitz plot analysis has large uncertainties, as do the background and efficiency simulations (due to limited numbers of MC events), so the method is tested on a range of different Dalitz plot models.

Pseudo-experiments with large numbers of events are used to investigate how CPV would be observed in the Dalitz plot. These experiments are simple "toy" simulations that produce points in the Dalitz plot according to the probability density function determined from the CLEO-c amplitude model with no representation of the proton-proton collision, detector, or trigger. Figure 3(a) illustrates the values of $\mathcal{S}_{CP}^i$ observed with 8×10^7 events and no CPV. This data set is approximately 50 times larger than the data sample under study. The resulting χ^2/ndf is 253.4/218, giving a p-value for consistency with no CPV of 5.0%. This test shows that the method by itself is very unlikely to yield false positive results. Figure 3(b) shows an example test using 5×10^7 events with a *CP* violating phase difference of 4° between the amplitudes for the $\phi(1020)\pi^+$ component in D^+ and D^- decays. The p-value in this case is less than 10^{-100}. The CPV effect is clearly visible, and is spread over a broad area of the plot,

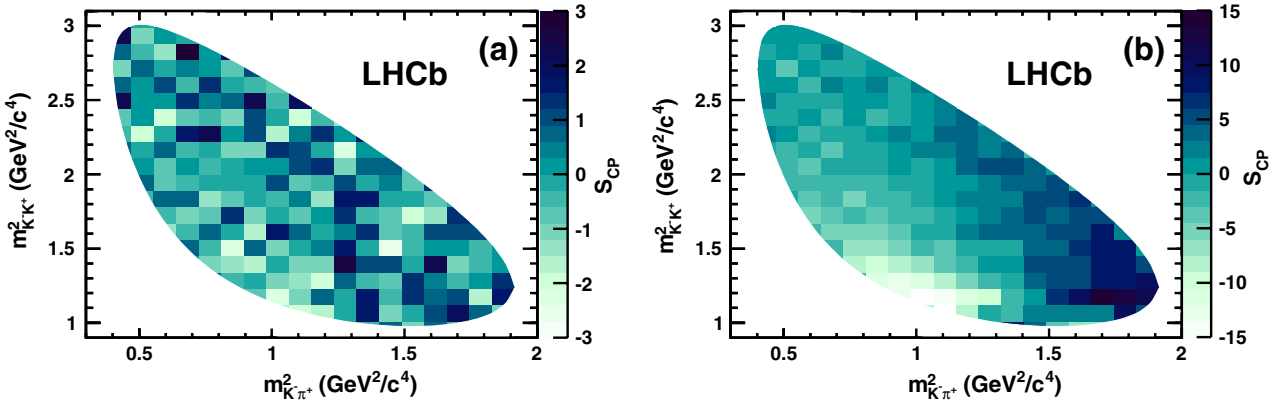

FIG. 3 (color online). $\mathcal{S}_{CP}$ across the Dalitz plot in a Monte Carlo pseudo-experiment with a large number of events with (a) no CPV and (b) a 4° CPV in the $\phi\pi$ phase. Note the difference in color scale between (a) and (b).

TABLE IV. Results from sets of 100 pseudo-experiments with different *CP* asymmetries and Adaptive I and II binnings. $p(3\sigma)$ is the probability of a 3σ observation of CPV. $\langle S\rangle$ is the mean significance with which CPV is observed.

CPV	Adaptive I		Adaptive II	
	$p(3\sigma)$	$\langle S\rangle$	$p(3\sigma)$	$\langle S\rangle$
No CPV	0	0.84σ	1%	0.84σ
6° in $\phi(1020)$ phase	99%	7.0σ	98%	5.2σ
5° in $\phi(1020)$ phase	97%	5.5σ	79%	3.8σ
4° in $\phi(1020)$ phase	76%	3.8σ	41%	2.7σ
3° in $\phi(1020)$ phase	38%	2.8σ	12%	1.9σ
2° in $\phi(1020)$ phase	5%	1.6σ	2%	1.2σ
6.3% in $\kappa(800)$ magnitude	16%	1.9σ	24%	2.2σ
11% in $\kappa(800)$ magnitude	83%	4.2σ	95%	5.6σ

changing sign from left to right. This sign change means the CPV causes only a 0.1% difference in the total decay rate between D^+ and D^-. This illustrates the strength of our method, as the asymmetry would be much more difficult to detect in a measurement that was integrated over the Dalitz plot. Even with no systematic uncertainties, to see a 0.1% asymmetry at the 3σ level would require 2.25×10^6 events. With the method and much smaller data set used here we would observe this signal at the 3σ level with 76% probability, as shown in Table IV below.

The sensitivity to a particular manifestation of CPV depends on the choice of binning. The fact that the *CP*-violating region in most of the pseudo-experiments covers a broad area of the Dalitz plot suggests that the optimal number of bins for this type of asymmetry is low. Each bin adds a degree of freedom without changing the χ^2 value for consistency with no CPV. However, if *CP* asymmetries change sign within a bin, they will not be seen. Similarly, the sensitivity is reduced if only a small part of a large bin has any CPV in it. To avoid effects due to excessive fluctuations, bins that contain fewer than 50 candidates are not used anywhere in the analysis. Such bins are very rare.

The binnings are chosen to reflect the highly nonuniform structure of the Dalitz plot. A simple adaptive binning algorithm was devised to define binnings of approximately equal population without separating D^+ and D^-. Two binnings that are found to have good sensitivity to the simulated asymmetries contain 25 bins ("Adaptive I") arranged as shown in Fig. 4(a), and 106 bins ("Adaptive II") arranged as shown in Fig. 4(b). For Adaptive I, a simulation of the relative value of the strong phase across the Dalitz plot in the CLEO-c amplitude model is used to refine the results of the algorithm: if the strong phase varies significantly across a bin, *CP* asymmetries are more likely to change sign. Therefore the bin boundaries are adjusted to minimize changes in the strong phase within bins. The model-dependence of this simulation could, in principle, influence the binning and therefore the sensitivity to CPV, but it cannot introduce model-dependence into the final results as no artificial signal could result purely from the choice of binning. Two further binning schemes, "Uniform I" and "Uniform II," are defined. These use regular arrays of rectangular bins of equal size.

The adaptive binnings are used to determine the sensitivity to several manifestations of CPV. With 200 test experiments of approximately the same size as the signal sample in data, including no asymmetries, no *CP*-violating signals are observed at the 3σ level with Adaptive I or Adaptive II. The expectation is 0.3.

With the chosen binnings, a number of sets of 100 pseudo-experiments with different *CP*-violating asymmetries are produced. The probability of observing a given signal in either the $\phi(1020)$ or $\kappa(800)$ resonances with 3σ significance is calculated in samples of the same size as the data set. The results are given in Table IV. The CPV shows up both in the χ^2/ndf and in the width of the fitted $\mathcal{S}_{CP}$ distribution.

For comparison, the asymmetries in the ϕ phase and κ magnitude measured by the CLEO Collaboration using the same amplitude model were $(6 \pm 6^{+0+6}_{-2-2})°$ and $(-12 \pm 12^{+6+2}_{-1-10})\%$, [15] where the uncertainties are statistical, systematic and model-dependent, respectively.

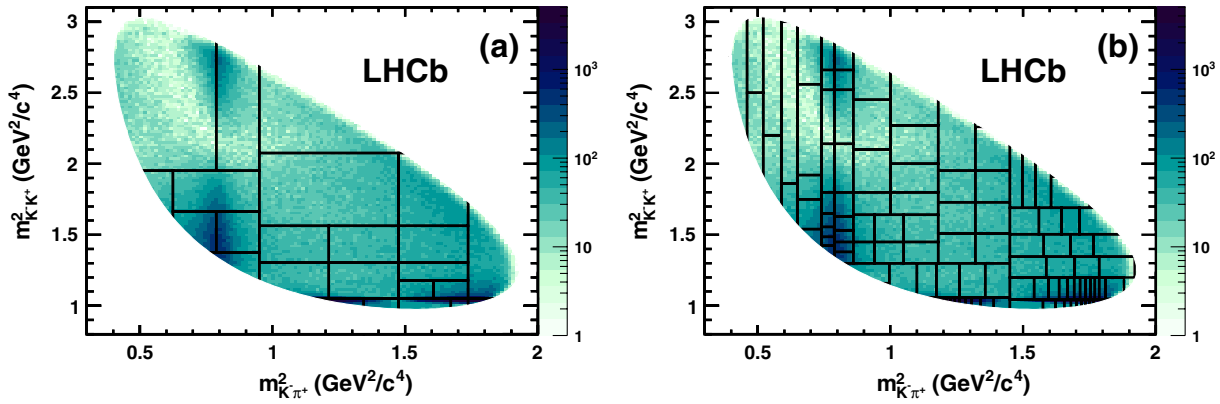

FIG. 4 (color online). Layout of the (a) "Adaptive I" and (b) "Adaptive II" binnings on the Dalitz plot of data.

TABLE V. Results from sets of 100 pseudo-experiments with 4° CPV in the $\phi(1020)$ phase and different Dalitz plot models. $p(3\sigma)$ is the probability of a 3σ observation of CPV. $\langle S\rangle$ is the mean significance with which CPV is observed. The sample size is comparable to that seen in data.

Model	Adaptive I		Adaptive II	
	$p(3\sigma)$	$\langle S\rangle$	$p(3\sigma)$	$\langle S\rangle$
B (baseline)	76%	3.8σ	41%	2.7σ
A	84%	4.3σ	47%	2.9σ
B2 (add $f_0(980)$)	53%	3.2σ	24%	2.2σ
B3 (vary $\bar{K}^*_0(1430)^0$ magn.)	82%	4.0σ	41%	2.8σ
B4 (vary $\bar{K}^*_0(1430)^0$ phase)	73%	3.7σ	38%	2.7σ

Table IV suggests that, assuming their model, we would be at least 95% confident of detecting the central values of these asymmetries.

The sensitivity of the results to variations in the Dalitz plot model and the background is investigated, and example results for the *CP* asymmetry in the $\phi(1020)$ phase are shown in Table V. In this table, models A and B are taken from the CLEO paper, model B2 includes an $f_0(980)$ contribution that accounts for approximately 8% of events, and models B3 and B4 are variations of the $\bar{K}^*_0(1430)^0$ amplitude and phase within their uncertainties. As expected, the sensitivity to CPV in the resonances of an amplitude model depends quite strongly on the details of the model. This provides further justification for our model-independent approach. However, a reasonable level of sensitivity is retained in all the cases we tested. Thus, when taken together, the studies show that the method works well. It does not yield fake signals, and should be sensitive to any large CPV that varies significantly across the Dalitz plot even if it does not occur precisely in the way investigated here.

IV. CONTROL MODES

It is possible that asymmetries exist in the data that do not result from CPV, for example, due to production, backgrounds, instrumental effects such as left-right differences in detection efficiency, or momentum-dependent differences in the interaction cross sections of the daughter particles with detector material. Our sensitivity to such asymmetries is investigated in the two Cabibbo favored control channels, where there is no large CPV predicted. The $D^+ \to K^-\pi^+\pi^+$ control mode has an order of magnitude more candidates than the Cabibbo-suppressed signal mode, and is more sensitive to detector effects since there is no cancellation between K^+ and K^- reconstruction efficiencies. Conversely, the $D_s^+ \to K^-K^+\pi^+$ control mode is very similar to our signal mode in terms of resonant structure, number of candidates, kinematics, detector effects, and backgrounds.

The control modes and their mass sidebands defined in Fig. 1 are tested for asymmetries using the method described in the previous section. Adaptive and uniform binning schemes are defined for $D^+ \to K^-\pi^+\pi^+$ and $D_s^+ \to K^-K^+\pi^+$. They are applied to samples 1–3 and each magnet polarity separately. In the final results, the asymmetries measured in data taken with positive and negative magnet polarity are combined in order to cancel left-right detector asymmetries. The precise number of bins chosen is arbitrary, but care is taken to use a wide range of tests with binnings that reflect the size of the data set for the decay mode under study.

For $D^+ \to K^-\pi^+\pi^+$, five different sets of bins in each scheme are used. A very low p-value would indicate a local asymmetry. One test with 25 adaptive bins in one of the subsamples (with negative magnet polarity) has a p-value of 0.1%, but when combined with the positive polarity sample the p-value increases to 1.7%. All other tests yield p-values ranging from 1–98%. Some example results are given in Table VI. A typical distribution of the $\mathcal{S}_{CP}$ values with a Gaussian fit is shown in Fig. 5(a) for a test with 900 uniform bins. The fitted values of the mean and width are consistent with one and zero, respectively, suggesting that the differences between the D^+ and the D^- Dalitz plots are driven only by statistical fluctuations.

For the $D_s^+ \to K^-K^+\pi^+$ mode a different procedure is followed due to the smaller sample size and to the high density of events along the ϕ and the $\bar{K}^*(892)^0$ bands. The Dalitz plot is divided into three zones, as shown in Fig. 6. Each zone is further divided into 300, 100 and 30 bins of same size. The results are given in Table VII. In addition, a test is performed on the whole Dalitz plot using 129 bins chosen by the adaptive algorithm, and a version of the 25-bin scheme outlined in Sec. III scaled by the ratio of the available phase space in the two modes. These tests yield p-values of 71.5% and 34.3%, respectively.

Other possible sources of local charge asymmetry in the signal region are the charm contamination of the background, and asymmetries from CPV in misreconstructed B decays. In order to investigate the first possibility, similar tests are carried out in the mass sidebands of the $D_{(s)}^+ \to K^-K^+\pi^+$ signal (illustrated in Fig. 1). There is no evidence for asymmetries in the background.

From a simulation of the decay $D^+ \to K^-\pi^+\pi^+$ the level of secondary charm ($B \to DX$) in our selected sample is found to be 4.5%. The main discriminating variable to

TABLE VI. Results (p-values, in %) from tests with the $D^+ \to K^-\pi^+\pi^+$ control channel using the uniform and adaptive binning schemes. The values correspond to tests performed on the whole data set in the mass windows defined in Sec. II.

	1300 bins	900 bins	400 bins	100 bins	25 bins
Uniform	73.8	17.7	72.6	54.6	1.7
Adaptive	81.7	57.4	65.8	30.0	11.8

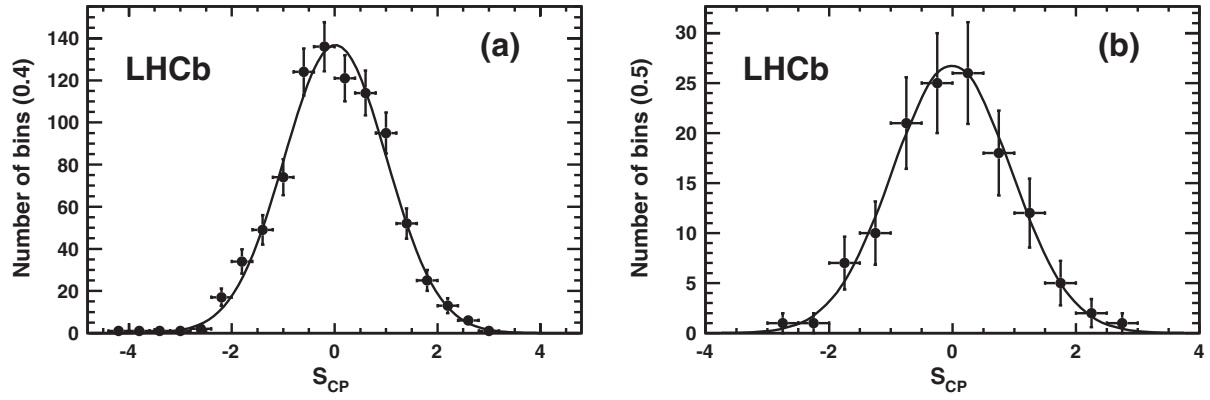

FIG. 5. (a) Distribution of $\mathcal{S}_{CP}$ values from $D^+ \to K^-\pi^+\pi^+$ from a test with 900 uniform bins. The mean of the fitted Gaussian distribution is 0.015 ± 0.034 and the width is 0.996 ± 0.023. (b) Distribution of $\mathcal{S}_{CP}$ values from $D_s^+ \to K^-K^+\pi^+$ with 129 bins. The fitted mean is -0.011 ± 0.084 and the width is 0.958 ± 0.060.

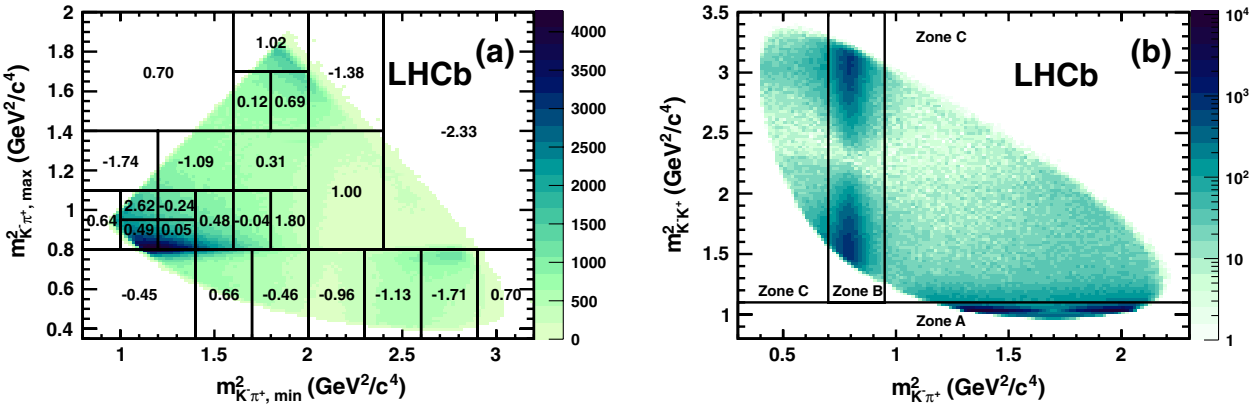

FIG. 6 (color online). Dalitz plots of (a) $D^+ \to K^-\pi^+\pi^+$, showing the 25-bin adaptive scheme with the $\mathcal{S}_{CP}$ values, and (b) $D_s^+ \to K^-K^+\pi^+$, showing the three regions referred to in the text. The higher and lower $K^-\pi^+$ invariant mass combinations are plotted in (a) as there are identical pions in the final state.

distinguish between prompt and secondary charm is the impact parameter (IP) of the D with respect to the primary vertex. Given the long B lifetime, the IP distribution of secondary charm candidates is shifted towards larger values compared to that of prompt D^+ mesons.

The effect of secondary charm is investigated by dividing the data set according to the value of the candidate IP significance ($\chi^2_{\rm IP}$). The subsamples with events having larger $\chi^2_{\rm IP}$ are likely to be richer in secondary charm. The results are shown in Table VIII. No anomalous effects are seen in the high $\chi^2_{\rm IP}$ sample, so contamination from secondary charm with CPV does not affect our results for studies with our current level of sensitivity.

The analysis on the two control modes and on the sidebands in the final states $K^-K^+\pi^+$ and $K^-\pi^+\pi^+$ gives results from all tests that are fully consistent with no asymmetry. Therefore, any asymmetry observed in $D^+ \to K^-K^+\pi^+$ is likely to be a real physics effect.

TABLE VII. Results (p-values, in %) from tests with the $D_s^+ \to K^-K^+\pi^+$ control channel using the uniform binning scheme. The values correspond to tests performed separately on Zones A–C, with samples 1–3 and both magnet polarities combined.

bins	Zone A	Zone B	Zone C
300	20.1	25.3	14.5
100	41.7	84.6	89.5
30	66.0	62.5	24.6

TABLE VIII. Results (p-values, in %) from tests with the $D^+ \to K^-\pi^+\pi^+$ and $D_s^+ \to K^-K^+\pi^+$ samples divided according to the impact parameter with respect to the primary vertex. The tests are performed using the adaptive binning scheme with 25 bins.

	$\chi^2_{\rm IP} < 6$	$\chi^2_{\rm IP} > 6$
$D^+ \to K^-\pi^+\pi^+$	8.5	88.9
$D_s^+ \to K^-K^+\pi^+$	52.0	30.6

TABLE IX. Fitted means and widths, χ^2/ndf and p-values for consistency with no CPV for the $D^+ \to K^-K^+\pi^+$ decay mode with four different binnings.

Binning	Fitted mean	Fitted width	χ^2/ndf	p-value (%)
Adaptive I	0.01 ± 0.23	1.13 ± 0.16	32.0/24	12.7
Adaptive II	-0.024 ± 0.010	1.078 ± 0.074	123.4/105	10.6
Uniform I	-0.043 ± 0.073	0.929 ± 0.051	191.3/198	82.1
Uniform II	-0.039 ± 0.045	1.011 ± 0.034	519.5/529	60.5

V. RESULTS

The signal sample with which we search for *CP* violation consists of 403 894 candidates selected within the $K^-K^+\pi^+$ mass window from 1856.7 to 1882.1 MeV/c^2, as described in Sec. II. There are 200 336 and 203 558 D^+ and D^- candidates, respectively. This implies a normalization factor $\alpha = N_{\rm tot}(D^+)/N_{\rm tot}(D^-) = 0.984 \pm 0.003$, to be used in Eq. (1).

The strategy for looking for signs of localized CPV is discussed in the previous sections. In the absence of local asymmetries in the control channels $D^+ \to K^-\pi^+\pi^+$ and $D_s^+ \to K^-K^+\pi^+$ and in the sidebands of the $K^-K^+\pi^+$ mass spectrum, we investigate the signal sample under different binning choices.

First, the adaptive binning is used with 25 and 106 bins in the Dalitz plot as illustrated in Fig. 4. Then CPV is investigated with uniform binnings, using 200 and 530 bins of equal size. For each of these binning choices, the significance $\mathcal{S}^i_{CP}$ of the difference in D^+ and D^- population is computed for each bin i, as defined in Eq. (1). The χ^2/ndf $= \sum_i (\mathcal{S}^i_{CP})^2$/ndf is calculated and the p-value is obtained. The distributions of $\mathcal{S}^i_{CP}$ are fitted to Gaussian functions.

The p-values are shown in Table IX. The Dalitz plot distributions of $\mathcal{S}^i_{CP}$ are shown in Fig. 7. In Fig. 8 the distributions of $\mathcal{S}^i_{CP}$ and the corresponding Gaussian fits for the different binnings are shown. The p-values obtained indicate no evidence for CPV. This is corroborated by the good fits of the $\mathcal{S}^i_{CP}$ distributions to Gaussians, with means and widths consistent with 0 and 1, respectively.

As further checks, many other binnings are tested. The number of bins in the adaptive and uniform binning schemes is varied from 28 to 106 and from 21 to 530,

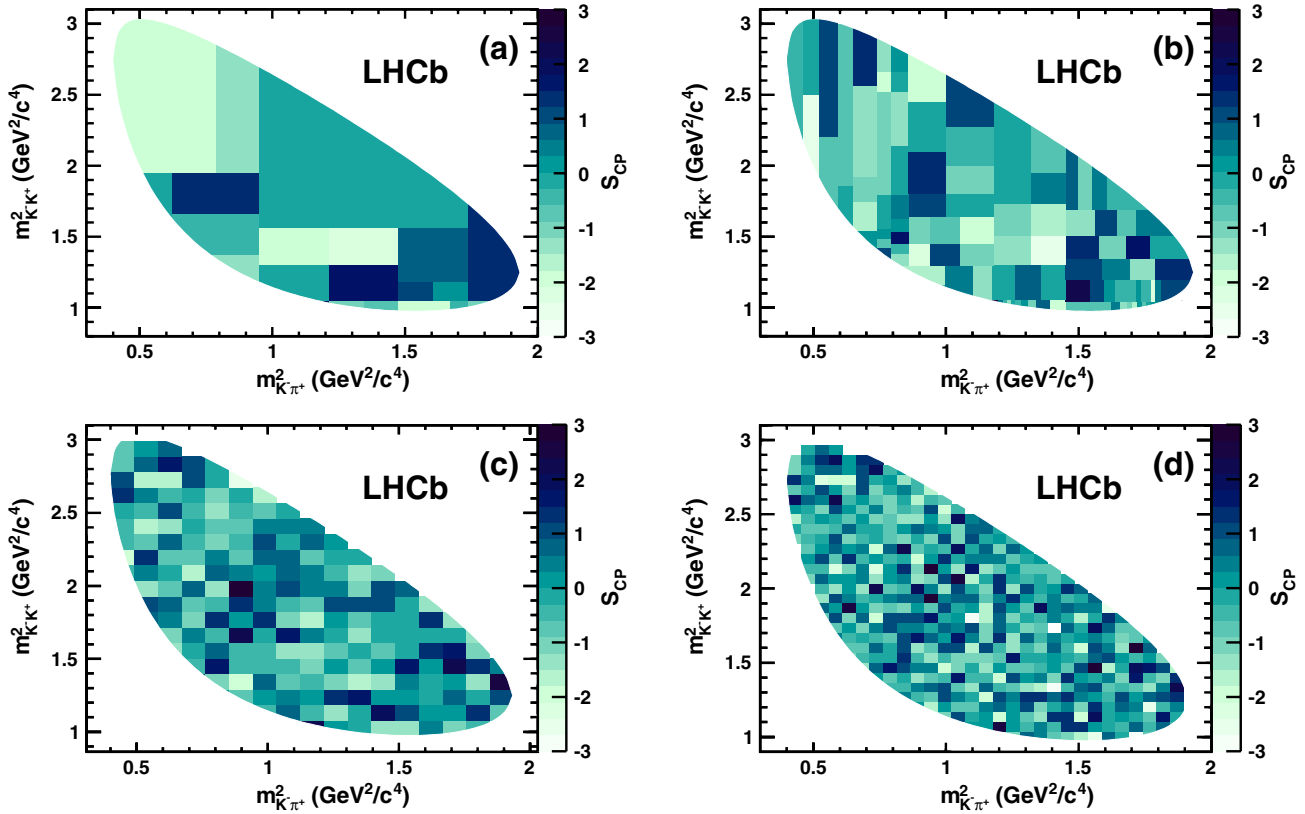

FIG. 7 (color online). Distribution of $\mathcal{S}^i_{CP}$ in the Dalitz plot for (a) "Adaptive I," (b) "Adaptive II," (c) "Uniform I" and (d) "Uniform II." In (c) and (d) bins at the edges are not shown if the number of entries is not above a threshold of 50 (see Sec. III).

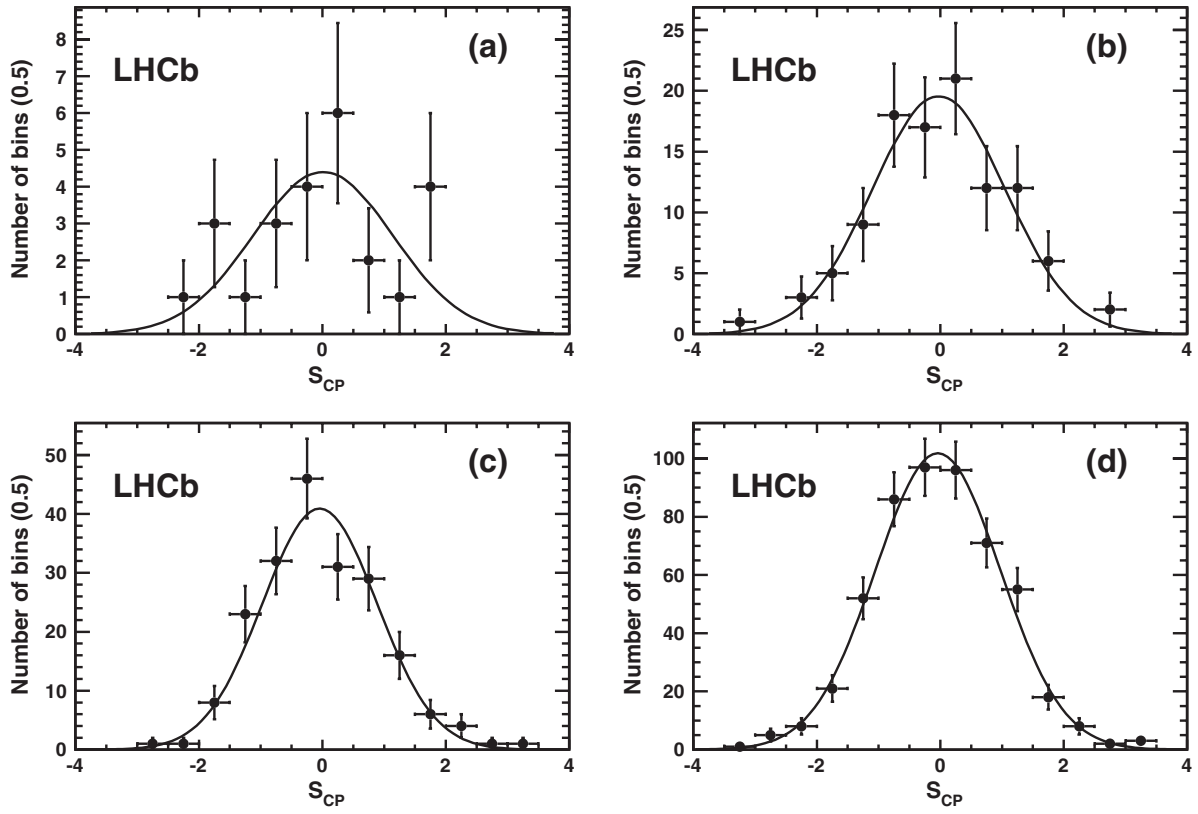

FIG. 8. Distribution of $\mathcal{S}^i_{CP}$ fitted to Gaussian functions, for (a) "Adaptive I," (b) "Adaptive II," (c) "Uniform I" and (d) "Uniform II." The fit results are given in Table IX.

respectively. The samples are separated according to the magnet polarity and the same studies are repeated. In all cases the p-values are consistent with no CPV, with values ranging from 4% to 99%. We conclude that there is no evidence for CPV in our data sample of $D^+ \to K^-K^+\pi^+$.

VI. CONCLUSION

Because of the rich structure of their Dalitz plots, three-body charm decays are sensitive to CP violating phases within and beyond the standard model. Here, a model-independent search for direct CP violation is performed in the Cabibbo-suppressed decay $D^+ \to K^-K^+\pi^+$ with 35 pb^{-1} of data collected by the LHCb experiment, and no evidence for CPV is found. Several binnings are used to compare normalized D^+ and D^- Dalitz plot distributions. This technique is validated with large numbers of simulated pseudo-experiments and with Cabibbo favored control channels from the data: no false positive signals are seen. To our knowledge this is the first time a search for CPV is performed using adaptive bins which reflect the structure of the Dalitz plot.

Monte Carlo simulations illustrate that large localized asymmetries can occur without causing detectable differences in integrated decay rates. The technique used here is shown to be sensitive to such asymmetries. Assuming the decay model, efficiency parameterization and background model described in Sec. III we would be 90% confident of seeing a CP violating difference of either 5° in the phase of the $\phi\pi^+$ or 11% in the magnitude of the $\kappa(800)K^+$ with 3σ significance. Since we find no evidence of CPV, effects of this size are unlikely to exist.

ACKNOWLEDGMENTS

We express our gratitude to our colleagues in the CERN accelerator departments for the excellent performance of the LHC. We thank the technical and administrative staff at CERN and at the LHCb institutes, and acknowledge support from the National Agencies: CAPES, CNPq, FAPERJ and FINEP (Brazil); CERN; NSFC (China); CNRS/IN2P3 (France); BMBF, DFG, HGF and MPG (Germany); SFI (Ireland); INFN (Italy); FOM and NWO (Netherlands); SCSR (Poland); ANCS (Romania); MinES of Russia and Rosatom (Russia); MICINN, XuntaGal and GENCAT (Spain); SNSF and SER (Switzerland); NAS Ukraine (Ukraine); STFC (United Kingdom); NSF (USA). We also acknowledge the support received from the ERC under FP7 and the Region Auvergne.

[1] N. Cabibbo, Phys. Rev. Lett. **10**, 531 (1963).
[2] M. Kobayashi and T. Maskawa, Prog. Theor. Phys. **49**, 652 (1973).
[3] S. Bianco, F. L. Fabbri, D. Benson, and I. Bigi, Riv. Nuovo Cimento Soc. Ital. Fis. **26N7**, 1 (2003).
[4] M. Artuso, B. Meadows, and A. A. Petrov, Annu. Rev. Nucl. Part. Sci. **58**, 249 (2008).
[5] Y. Grossman, A. L. Kagan, and Y. Nir, Phys. Rev. D **75**, 036008 (2007).
[6] Throughout this paper charge conjugation is implied, unless otherwise stated.
[7] B. Aubert *et al.* (*BABAR* Collaboration), Phys. Rev. D **71**, 091101 (2005).
[8] P. Rubin *et al.* (CLEO Collaboration), Phys. Rev. D **78**, 072003 (2008).
[9] M. Staricˆ *et al.* (Belle Collaboration), arXiv:1110.0694.
[10] I. Bediaga, I. Bigi, A. Gomes, G. Guerrer, J. Miranda *et al.*, Phys. Rev. D **80**, 096006 (2009).
[11] B. Aubert *et al.* (*BABAR* Collaboration), Phys. Rev. D **78**, 051102 (2008).
[12] L. Lyons, *Statistics for Nuclear and Particle Physicists* (Cambridge University Press, Cambridge, England, 1989), ISBN 978052137934.
[13] A. Alves *et al.* (LHCb Collaboration), JINST **3**, S08005 (2008).
[14] S. Agostinelli *et al.* (GEANT4 Collaboraton), Nucl. Instrum. Methods Phys. Res., Sect. A **506**, 250 (2003).
[15] The conventions used in the CLEO paper to define asymmetry are different, so the asymmetries in Table II of [8] have been multiplied by two in order to be comparable with those given above.